WFC3 Instrument Science Report 2011-02

# WFC3/UVIS Charge Injection Behavior: Results of an Initial Test

H. Bushouse, S. Baggett, R. Gilliland, K. Noeske, L. Petro
January 07, 2011

**ABSTRACT**

*The WFC3 CCD Charge Injection (CI) capability has been tested on-orbit in Cycle18 calibration program 12348. Bias, dark, and science exposures of star cluster NGC 104 have been obtained in all commandable CI modes. Super-bias images were constructed for each CI mode and used to calibrate the NGC 104 exposures. Analysis has shown that the CI mode is working as expected, producing injected signals of ~15000 $e^-$/pix. The CI signal is stable and repeatable to a level of a few $e^-$/pix. CI rows in calibrated science images have mean residual signals of a few $e^-$/pix with 1-sigma noise of ~18 $e^-$/pix. Noise in science images in the rows in between CI varies from 3.5-6.5 $e^-$/pix, compared to ~3.4 $e^-$/pix in non-CI images.*

## Introduction

The cycle 18 WFC3 calibration program 12348 was executed in preparation for making the CCD charge injection (CI) capability available to observers in cycle 19, which can be used to mitigate the effects of Charge Transfer Efficiency (CTE) degradation in the CCDs. The program was used to confirm that the CI performs on-orbit as it did during ground testing, to provide an initial assessment of which CI mode is most effective at mitigating CTE losses, and to obtain a baseline calibration for each CI mode. To fulfill these goals, the program obtained bias and dark exposures in each CI mode, and also obtained observations of NGC 104 (47 Tucanae) in each of the CI modes, which are being used to evaluate the photometric benefits of CI.

This report focuses on an analysis of the characteristics and behavior of the charge injection itself. Future reports will present the results of photometric measurements of the NGC 104 cluster. These will include comparisons of the results for normal and charge injected images, in order to determine the effectiveness of CI at mitigating CTE losses.

## Observations

Program 12348 consisted of a total of 45 visits, which were all executed between September 27 and October 4, 2010. Five one-orbit visits were devoted to observations in the outskirts (6' west of the center) of NGC 104, where the exposures in one visit used no CI, and the remaining four each used one of the available CI modes. The four available CI modes are: 1) continuous, where every line of the CCD receives injected charge; 2) LINE10, where every $10^{th}$ line contains injected charge; 3) LINE17, where every $17^{th}$ line contains injected charge; and 4) LINE25, where every $25^{th}$ line contains injected charge. A total of eight exposures were obtained in each visit for NGC 104, distributed as two short (30 sec) and two long (360 sec) exposures at each of two pointings. The two pointings were offset by one CCD chip width, which is half the WFC3 UVIS field of view. The exposures within each pair of long and short exposures were also dithered by a small amount (~2.5 pixels) in each direction, in order to allow for cosmic-ray and bad pixel rejection. The F502N filter was used for the NGC 104 exposures in order to minimize sky background and therefore maximize charge transfer inefficiency effects.

The remaining visits of the program were devoted to obtaining bias and dark exposures in each of the four CI modes. The plan was to obtain a total of 23 biases and 10 darks (900 sec each) for each CI mode. Due to a safing incident on October 4, however, some of the very last exposures in the program were lost, resulting in a total of 21 biases and 9 darks for continuous mode, 19 biases and 9 darks for LINE10, 23 biases and 10 darks for LINE17, and 19 biases and 9 darks for LINE25 mode. Table 1 lists the type of observations in each visit of the program.

**Table 1: Summary of program 12348 observations**

| Visit(s) | Target | CI Mode |
|---|---|---|
| 01 | NGC 104 | none |
| 02 | NGC 104 | Continuous |
| 03 | NGC 104 | LINE10 |
| 04 | NGC 104 | LINE17 |
| 05 | NGC 104 | LINE25 |
| 30-39 | Bias & Dark | Continuous |
| 40-49 | Bias & Dark | LINE10 |
| 50-59 | Bias & Dark | LINE17 |
| 60-69 | Bias & Dark | LINE25 |

## Data Reduction

All of the bias exposures were processed with calwf3 to perform overscan bias subtraction using the BLEVCORR calibration step. The overscan-subtracted biases for each CI mode were then combined to form a super-bias, which was done using the IRAF task "imcombine". The combined images were formed by applying 3-sigma rejection and taking the median of the remaining values at each pixel. The combined images were reformatted into bias reference files, using the standard deviation about the median at each pixel (as computed by imcombine) to fill the ERR extensions of the reference files. The NGC 104 observations were then reprocessed with

calwf3, using the appropriate CI mode super-biases for the exposures that used CI. The resulting calibrated images have the overall CI pattern subtracted from them. For the NGC 104 observations that were obtained without CI, we used a comparable super-bias that was created from the combination of 19 bias exposures from the WFC3 UVIS calibration program 11905. The normal bias exposures were obtained over the same range of dates as the CI biases.

## Charge Injection Behavior

We have used the charge-injected biases and darks, as well as the CI bias-subtracted images of NGC 104, to analyze various characteristics and the behavior of the CI itself in each of the four modes. First, in order to help orient the reader, in Figure 1 we show an example of a bias image taken with LINE10 mode CI turned on. Only a small portion of the full image is shown. The CI signal appears in every $10^{th}$ horizontal row. The figure shows exposures taken during ground testing and on-orbit. Notice how the CTE degradation that has already occurred in the first 16 months on orbit causes some of the CI signal to be trailed into the image rows in between the CI lines during the readout process.

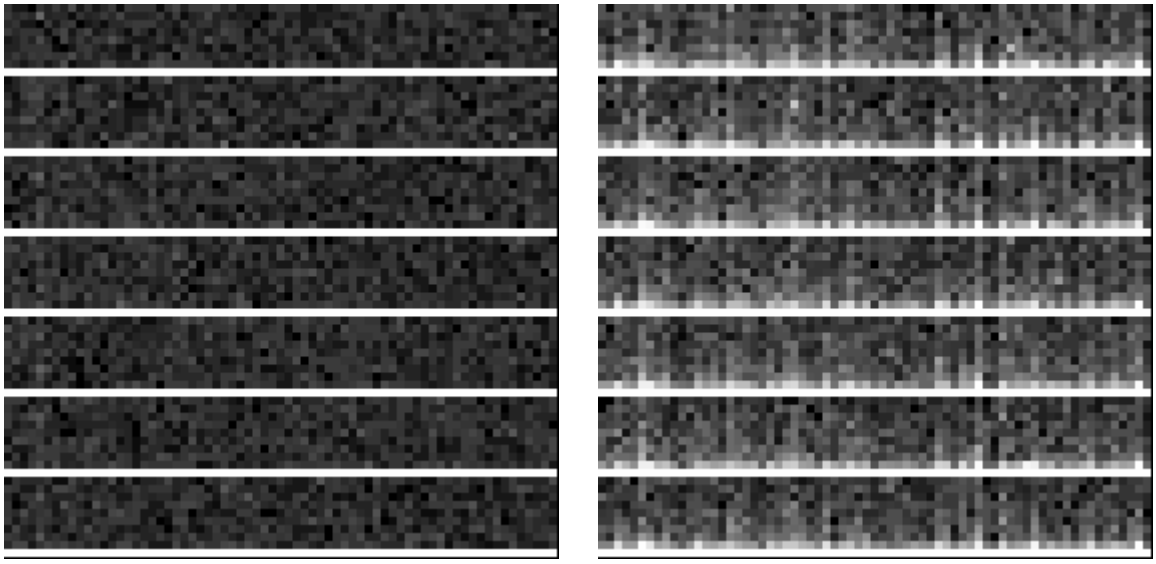

**Figure 1: Small portions of LINE10 mode charge injected bias images. The intensity stretch is chosen to highlight the pixel values between the CI lines. The image on the left was obtained during ground thermal-vacuum tests, while the one on the right is from the on-orbit cal program 12348.**

The CI signal level varies a bit amongst the four amplifier quadrants of the CCDs, ranging from about 13000-17000 $e^-$/pix above the overall bias level. Figure 2 shows the average CI signal level in each of the injected rows of CCD chip 2 for all four CI modes. For the LINE modes the signal decreases with distance from the readout amps, while the continuous mode appears to be self-correcting for CTE losses. The chip 1 behavior is the same.

The continous CI mode has an unexpected behavior in that every $10^{th}$ row has a mean CI signal level that is depressed by 6-7 DN, as seen by the individual line of black points in Figure 2 that is offset below the rest of the data for the continous mode. It just so happens that the depressed rows are the same physical CCD rows that receive CI in the LINE10 mode, yet the

LINE10 mode itself does not appear to show any kind of anomalous behavior relative to the others. The cause of this is not understood at this time.

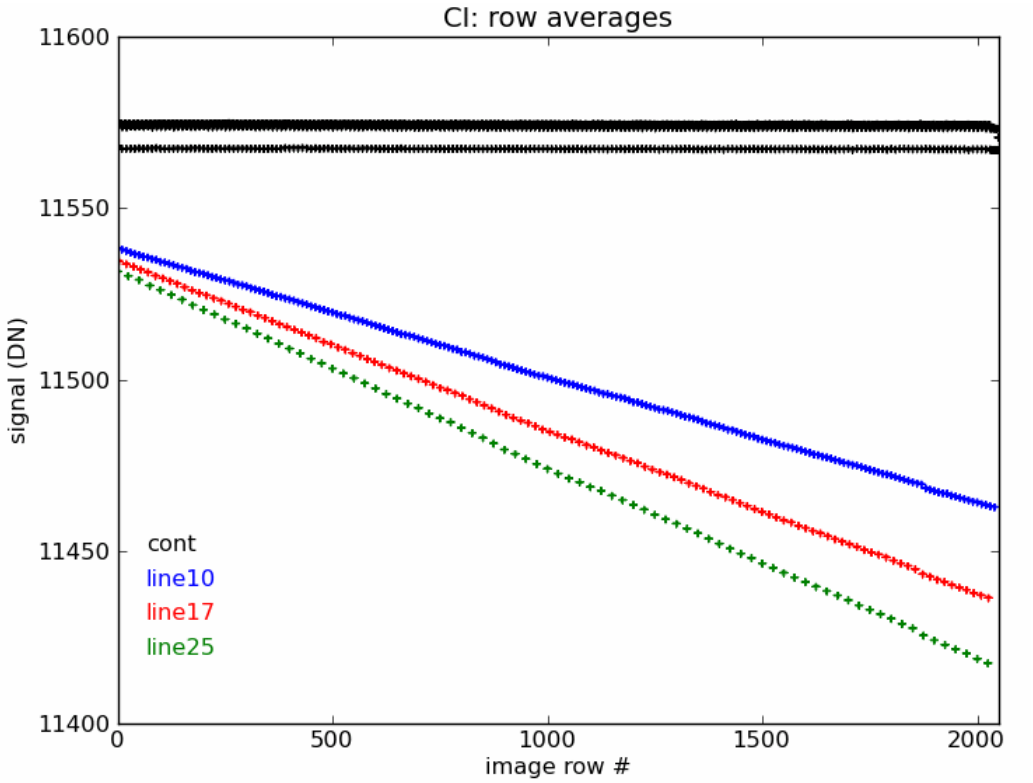


**Figure 2: Average CI signal level as a function of image row number for CCD chip 2. Row 1 is right next to the readout amps. Chip 1 behavior is the same.**

The average signal levels within rows between the CI lines are shown in Figures 3-5 for the LINE10, LINE17, and LINE25 modes, respectively. There is a clear decay of trapped signal in the rows trailing the CI at a level of a few DN per pixel.

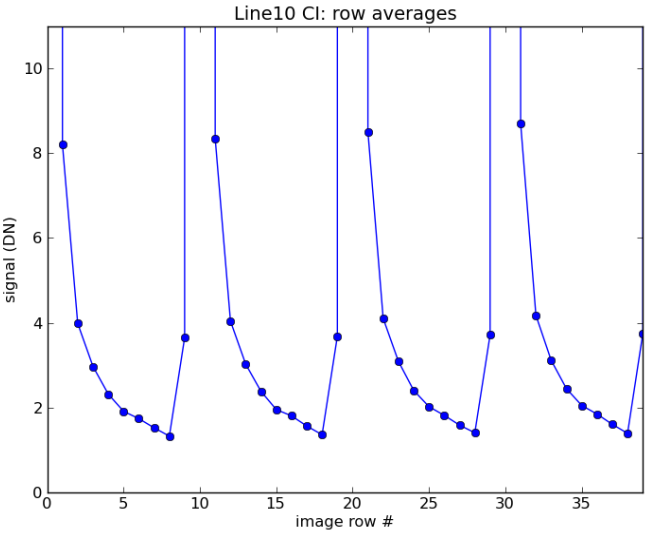


**Figure 3: Average signal per row in a LINE10 image. The CI lines themselves lie off the top of the plot.**

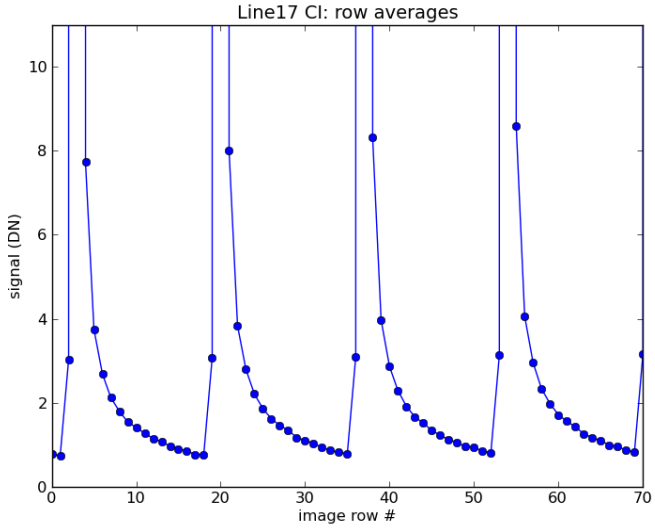


**Figure 4: Average signal per row in a LINE17 image.**

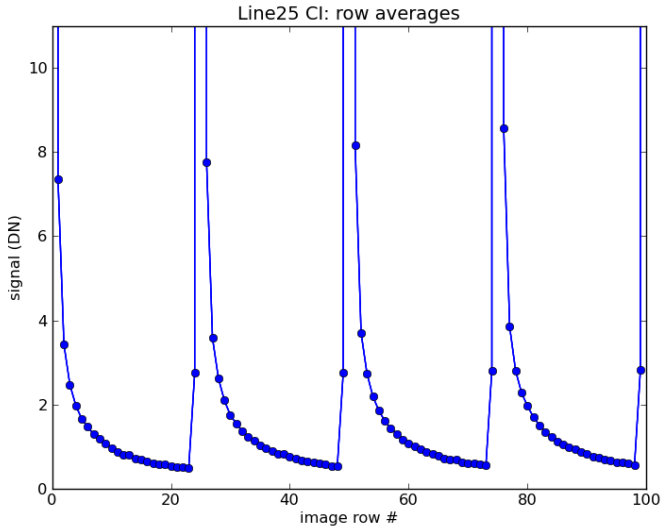


**Figure 5: Average signal per row in a LINE25 image.**

We have examined the stability of the CI signal in a number of ways. First, we have looked at the mean CI signal level as a function of time in rows 701 and 1551 of chip 2 for all of the CI biases that were taken. Rows 701 and 1551 are the only two CI rows that are common to all three LINE modes and were therefore chosen to get a consistent measure for the different modes. As can be seen from Figure 6, there is no significant dependence of CI signal level over time, at least within the rather limited seven day range of these observations. Another way to investigate the stability of the CI signal is to subtract the mean CI super-bias for a given mode from one of the individual biases and measure the residuals. In the rows of such a difference image that contained CI, the mean residual signal level is less than 1 $e^-$/pix, with residual noise along the row of 17-18 $e^-$/pix. FFT analysis of such residual images also shows no remaining structure at any frequency.

We also looked at the mean signal in the CI image rows as a function of WFC3 input voltage from the HST power bus, which is shown in Figure 7. There is again no indication of any

correlation between CI signal level and WFC3 input voltage, as the voltage varies within each HST orbit.

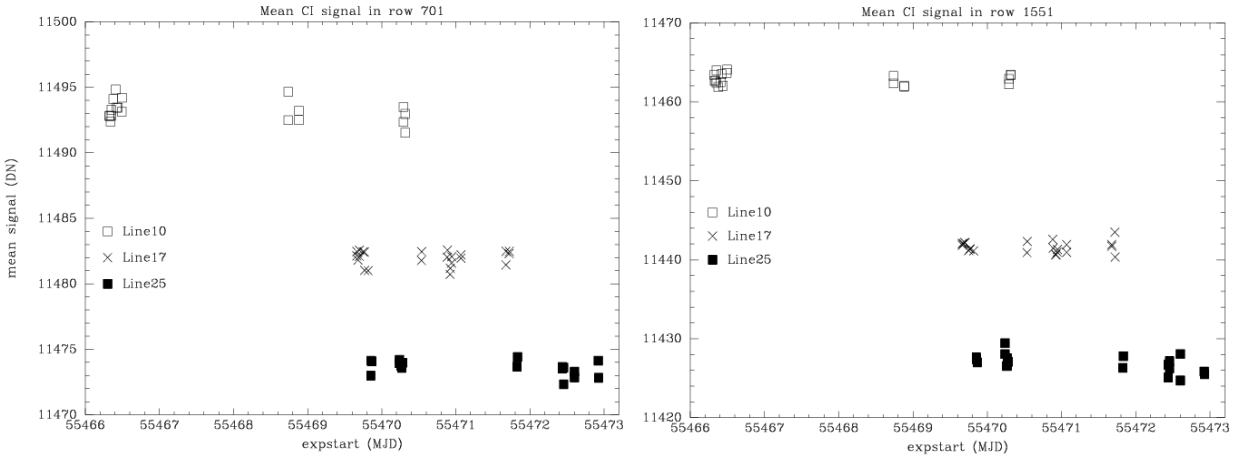


**Figure 6: Mean CI signal in rows 701 (left) and 1551 (right) of all LINE mode biases vs. exposure start time.**

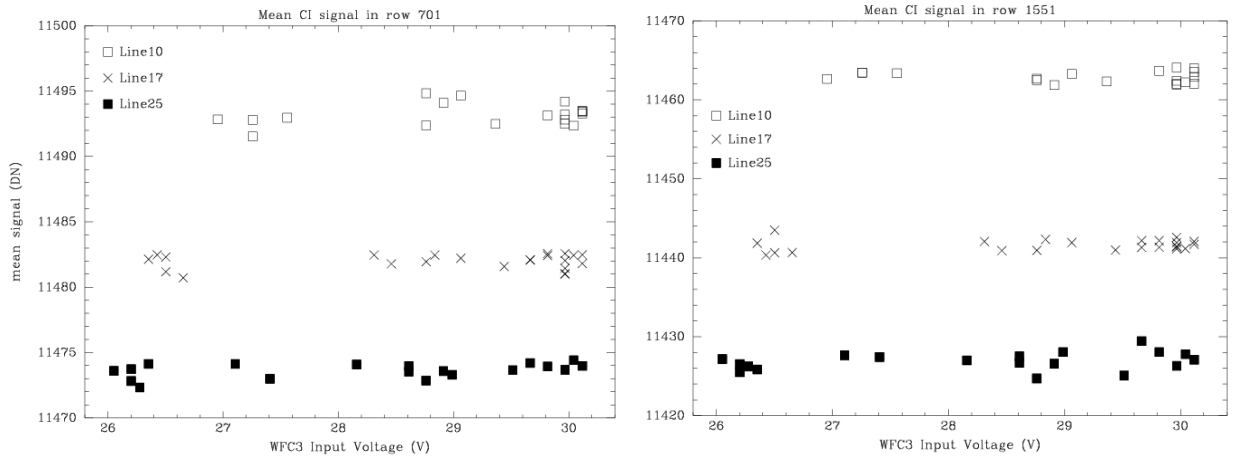


**Figure 7: Mean CI signal in rows 701 (left) and 1551 (right) of all LINE mode biases vs. WFC3 voltage**

The most important aspect of the CI behavior is of course the way it affects science exposures. We have analyzed several aspects of the NGC 104 exposures after reprocessing them with the CI super-biases. Figure 8 shows a small section of one of the NGC 104 exposures that used LINE10 CI. The left panel shows the calibrated image after subtraction of a regular (non-CI) bias during calwf3 calibration and therefore still has the CI signal in every 10$^{th}$ line, while the right panel shows the result after subtracting the LINE10 super-bias. The mean residual signal in the CI lines is a few $e^-$/pix, relative to the original CI signal of 13000-17000 $e^-$/pix. The noise in the CI-subtracted lines is 17-20 $e^-$/pix, which is of course significantly lower than what would result from the Poisson distribution of an equivalent signal at ~15000 $e^-$/pix. Figure 9 shows a plot of the mean residual signal in the CI-subtracted rows of a science image for each of the LINE modes. The residual signal is smallest at the edge of the chip next to the readout amps (row 1 in this case), and slowly grows to a few $e^-$/pix at the edge of the chip furthest from the amps.

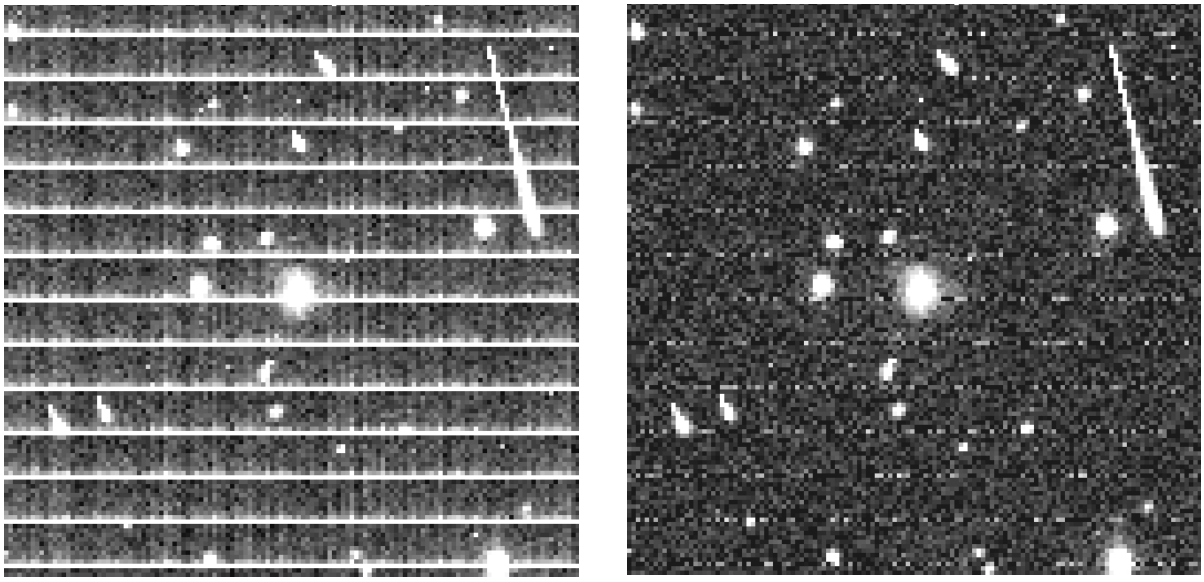

**Figure 8: Portion of an NGC 104 exposure without (left) and with (right) CI subtraction. Both images are shown with a hard intensity stretch to highlight the low-level CI signal residuals.**

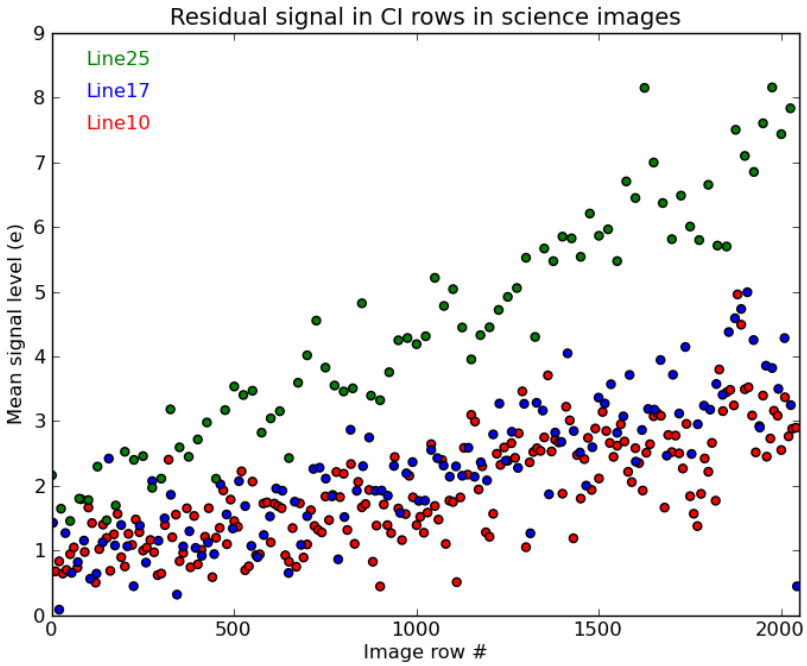


**Figure 9: Mean residual signal in CI-subtracted rows of science images for each LINE mode. Only the data for CCD chip 2 is shown; chip 1 behavior is the same.**

The small amount of CI signal that is trailed into the image rows in between the injected rows is removed well enough to not show any such trend (see Figure 10). More detailed views of the residual signal per row of CI-subtracted science images are shown in Figure 11 and Figure 12. Figure 11 shows the mean signal per row for one of the short (30 sec) exposures of NGC 104 that used LINE10 CI and has had a LINE10 bias image subtracted. Two sets of rows are shown: one set of 10 rows near the CCD readout amps (blue points) and another set of 10 rows on the far side of the chip (red points). The residual signal, averaged over the row, in the row that had CI

(row 1) is ~0.5 e⁻/pix. The residual signal in the 9 rows in between the CI is essentially zero, with no dependence on row number, which again indicates that the CI signal that was trailed into subsequent rows during the readout has been effectively removed. Figure 12 shows the same type of measurements for one of the long (360 sec) exposures of NGC 104, which also used LINE10 CI and has been CI-subtracted. In this case the longer exposure has resulted in an overall background level of ~0.5 e⁻/pix. The residual signal in the CI rows (row 1) is approximately +/- 1 e⁻/pix and the rows in between the CI again show no obvious residuals of the CI signal.

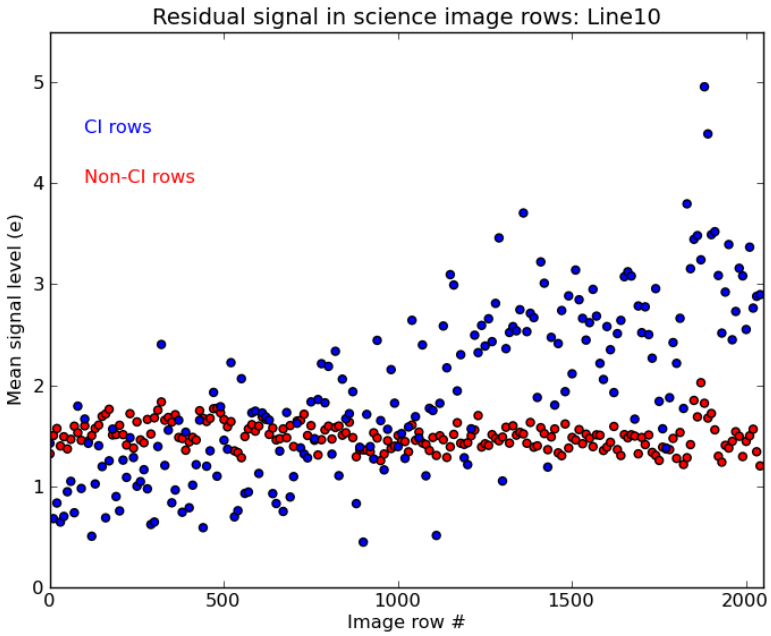


**Figure 10: Mean residual signal per row in a LINE10 science image. Only data for chip 2 is shown.**

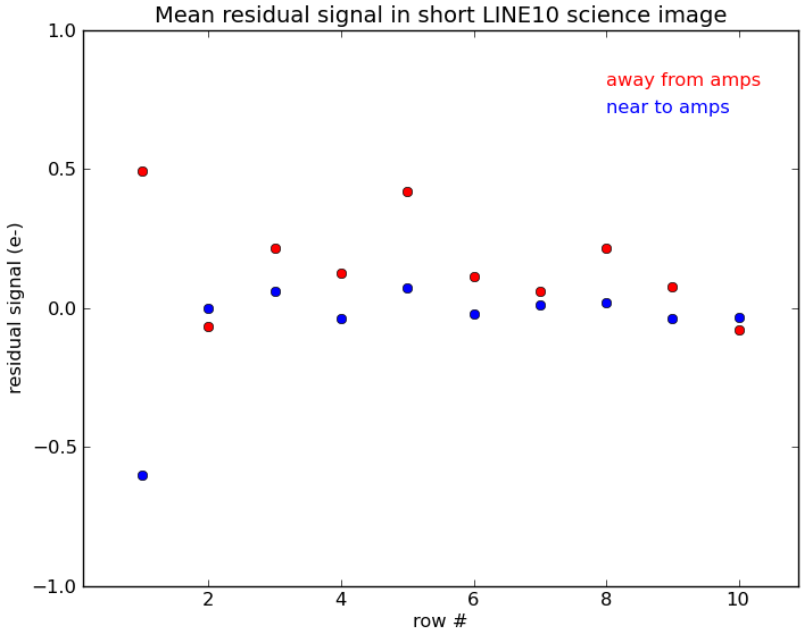


**Figure 11: Mean residual signal per row for two sets of 10 rows in a LINE10 image of NGC 104 that has had a CI bias subtracted. The short (30 sec) exposure time result in essentially zero background signal.**

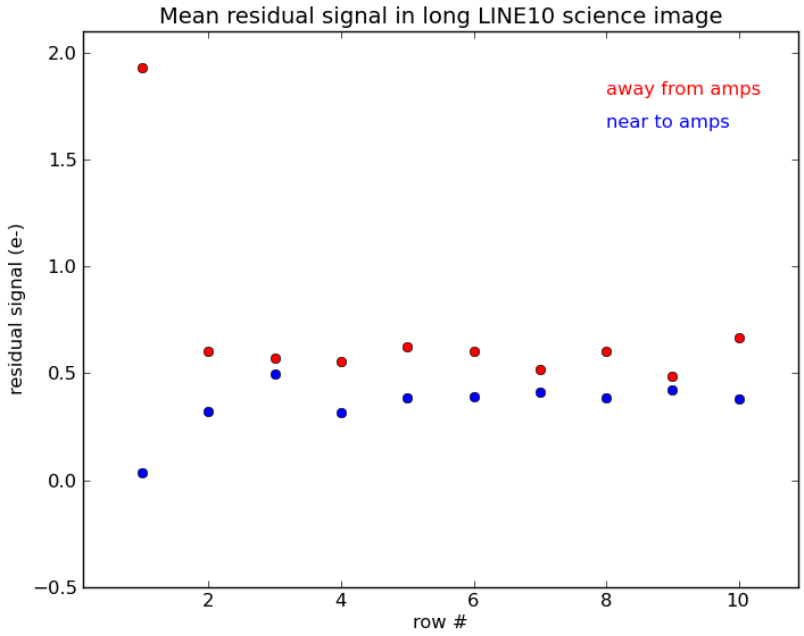


**Figure 12: Mean residual signal per row for two sets of 10 rows in a LINE10 image of NGC 104 that has had a CI bias subtracted. The longer exposure time for this image results in a background signal of ~0.5 $e^-$/pix.**

Another important aspect of CI-subtracted science images is the amount of residual noise in the image rows that had CI, as well as in the non-CI rows. Figure 13 shows the noise (one sigma about the mean) along each CI row of a LINE10 science image that has had a CI bias image subtracted from it. The noise in the CI rows ranges from 17-20 $e^-$/pix, being lowest in the rows closet to the readout amps for each chip and increasing with distance from the amps. LINE17 and LINE25 images show the same behavior with the same level of noise.

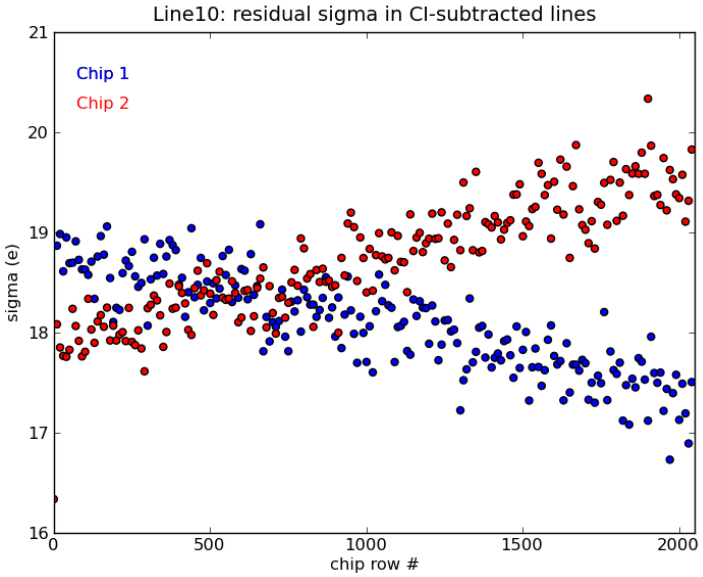


**Figure 13: Residual noise in CI-subtracted rows of a LINE10 science image.**

The amount of noise in image rows between the CI lines for LINE10, LINE17, and LINE25 bias-subtracted images is shown in Figures 14-16, respectively. Near the edges of the CCD chips that are furthest away from the readout amps the noise is ~6.5 $e^-$/pix in the image row immediately following a CI line, which gradually decays to 4-4.5 $e^-$/pix for the image rows furthest downstream of a CI line. For the side of a chip closest to the amps, the noise starts out at ~4.5 $e^-$/pix and declines to 3.5-4 $e^-$/pix. Notice that the noise level in these rows gradually approaches that of normal, non-CI images, but always remains just a bit higher, by a few tenths of an electron.

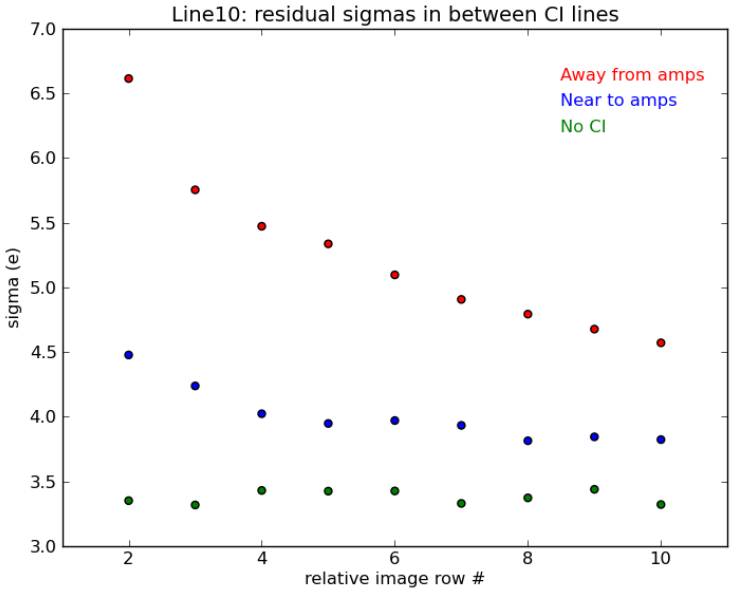


**Figure 14: Residual noise between CI lines in a LINE10 bias-subtracted image. The noise in the same lines of an image with no CI is included for comparison.**

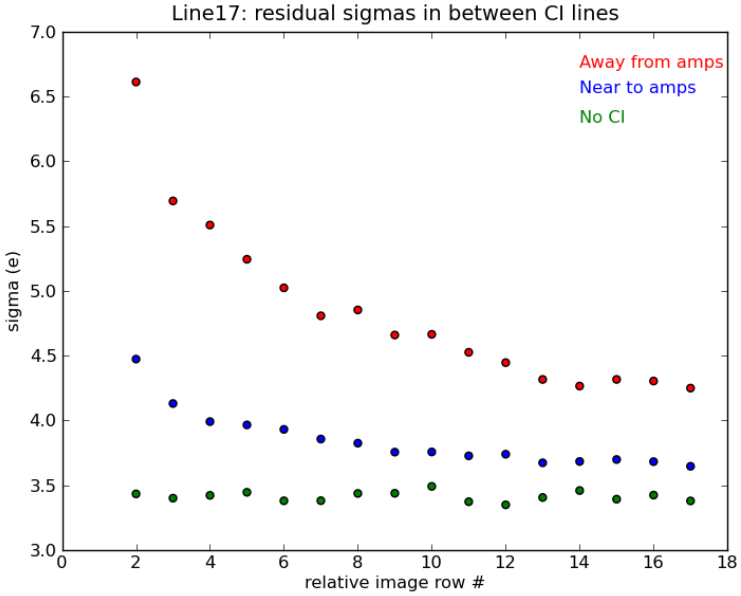


**Figure 15: Residual noise between CI lines in a LINE17 bias-subtracted image.**

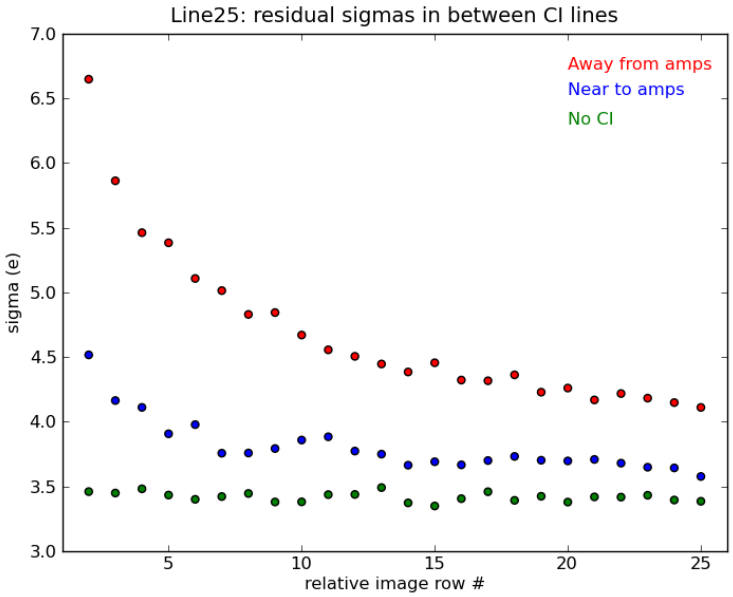


**Figure 16: Residual noise between CI lines in a LINE25 bias-subtracted image.**

## Conclusions

Initial analysis of the data from program 12348 has shown that the WFC3 CCD charge injection mode is working as expected for all commandable modes. The injection process results in a signal of ~15000 $e^-$/pix in the charge injected rows of the CCDs. For the discrete LINE modes of CI, the reduction in CTE that has already occurred since WFC3 was launched results in a small fraction of the CI signal being trailed into non-CI rows, at levels of 2-6 $e^-$/pix. The CI signal is stable to a level of a few $e^-$/pix from image to image, allowing for good subtraction of the CI pattern from science images through the use of a CI super-bias image. The CI signal level also shows no obvious dependence on the WFC3 instrument input voltage, which regularly varies during each orbital period of HST.

Science images – in this case observations of the star cluster NGC 104 – obtained with CI turned on show residual noise of ~18 $e^-$/pix in the CI rows after subtracting a CI super-bias, which is far lower than what would result from a Poissonian signal at the same level. The noise in calibrated science images in the rows in between CI varies as a function of distance from the CCD readout amplifiers and distance from the CI rows: near the amps the noise is 3.5-4.5 $e^-$/pix and gradually increases to 4.5-6.5 $e^-$/pix at the edge of the chip furthest from the amps. The lowest CI-subtracted noise levels are therefore only a few tenths of an $e^-$/pix higher than that in equivalent non-CI images. The average noise in CI-subtracted LINE10 mode images is ~4.5 $e^-$/pix, compared to ~3.4 $e^-$/pix in non-CI images. For readnoise-limited images, this implies a decrease in sensitivity to faint sources of a factor of ~1.8.